Neural signatures of reduced serial dependence in anti-NMDAR encephalitis and schizophrenia

Heike Stein[1,3], Joao Barbosa[1,3], Diego Lozano-Soldevilla[1], Mireia Rosa-Justicia[1], Alba Morató[1], Adrià Galan-Gadea[1], Laia Prades[1], Amaia Muñoz-Lopetegui[1,2], Helena Ariño[1,2], Eugenia Martinez-Hernandez[1,2], Mar Guasp[1,2], Josefina Castro-Fornieles[1,4,5], Josep Dalmau[1,2,5,6], Joan Santamaria[2], Albert Compte[1]

[1] Institut d'Investigacions Biomèdiques August Pi i Sunyer (IDIBAPS), Barcelona, Spain
[2] Service of Neurology, Hospital Clínic de Barcelona, Barcelona, Spain
[3] Laboratoire de Neurosciences Cognitives et Computationnelles, INSERM U960, Ecole Normale Supérieure - PSL Research University, Paris, France
[4] Department of Child and Adolescent Psychiatry and Psychology, CIBERSAM, Institute Clinic of Neurosciences, Hospital Clínic, Barcelona, Spain
[5] University of Barcelona, Barcelona, Spain
[6] Catalan Institution for Research and Advanced Studies (ICREA), Barcelona, Spain.

Abstract

Serial dependence, a behavioral phenomenon where information from previous trials biases current trial reports, is pervasive in working memory tasks. There is growing interest in its mechanisms, and recent work has shown that individuals with schizophrenia and anti-NMDA receptor (NMDAR) encephalitis exhibit reduced serial dependence in simple delayed-response tasks. Modeling and experimental evidence suggest that serial dependence stems from the interplay between persistent neural activity and short-term synaptic plasticity in cortical circuits, with neural reactivations in between trials increasing serial dependence. A computational model that implements this hypothesis showed that a reduction in short-term plasticity, potentially due to NMDAR dysfunction, can replicate the observed reduction of serial dependence in patients with anti-NMDAR encephalitis and schizophrenia, compared with healthy subjects. Yet, its neurophysiological predictions remain untested. Here, we used electroencephalography (EEG) to test if these patient groups have reduced neural reactivations, as the model predicts. Our findings confirm the absence of memory reactivations in schizophrenia and anti-NMDAR encephalitis. We show that this result does not depend on motor-related activity. Further, while memory codes are specifically impaired in these patients, the perceptual component of the code is as robust as in healthy participants. Overall, we report empirical evidence supporting a mechanistic model of serial dependence, which links reduced neural reactivations with diminished serial dependence in neuropsychiatric disorders.

Introduction

Working memory lies at the core of cognition (Conway et al., 2003), as it maintains information for short periods of time in a format that makes it easy to access and manipulate (Baddeley, 1992). Deficits in working memory play a particularly important role in the cognitive dysfunction characteristic of some psychiatric and neurological disorders, such as schizophrenia (Goldman-Rakic, 1994) or anti-NMDA-receptor (NMDAR) encephalitis (Dalmau et al., 2007; Guasp et al., 2022), in which they even form part of early diagnostic criteria (Graus et al., 2016). At the neurobiological level, it has been proposed that these deficits could be linked to the dysfunction of NMDARs in memory-maintaining circuits like the prefrontal cortex in both anti-NMDAR encephalitis and schizophrenia (Olney et al., 1999; Wang, 1999; Javitt, 2010). In line with this reasoning, we have recently reported a novel, qualitative alteration in working memory processing in patients with anti-NMDAR encephalitis and schizophrenia (Stein et al., 2020). Specifically, we showed that a history dependency of memory reports in a visuo-spatial working memory task (so-called serial dependence) was markedly reduced in both patient groups. Our finding has been replicated in independent cohorts of persons with schizophrenia (Bansal et al., 2023; Gold et al., 2023) and has been extended to perceptual decision making tasks as a possible behavioral biomarker of psychosis proneness in the general population (Eckert et al., 2023).

Serial dependence is a common phenomenon in neurotypical subjects performing structured laboratory tasks (Kiyonaga et al., 2017). It indicates that traces of memory information are carried over between subsequent working memory trials, even when this is not required to perform the task. After the memory report, circuits such as the prefrontal cortex usually cease to encode working memory items in persistent neural firing (Funahashi et al., 1989), which is the canonical mechanism of working memory maintenance (Goldman-Rakic, 1995). Hence, alternative mechanisms to persistent activity (Bliss and D'Esposito, 2017; Kilpatrick, 2018) or persistent activity in other brain regions (Akrami et al., 2018) have been proposed to represent previously memorized items between consecutive trials. Neurophysiological and computational modeling data support the view that a non-spiking mechanism in the prefrontal cortex, such as short-term synaptic plasticity (STP), could temporarily maintain stimulus-specific information throughout periods with no persistent tuning, such as the inter-trial interval (ITI), and bias memory reports in upcoming trials (Barbosa et al., 2020). Evidence for a STP mechanism holding information between trials was found in the monkey's prefrontal cortex, specifically in neuron-pair cross-correlation peaks that remained tuned to the recently memorized stimulus throughout the ITI, and in neural code reactivations just before the onset of a new stimulus (Barbosa et al., 2020). In a parallel human experiment, similar memory reactivations in alpha power extracted from human electroencephalography (EEG) were found, congruent with other work (Bae and Luck, 2019; Sheehan and Serences, 2022; Hajonides et al., 2023; Zhang and Luo, 2023). In both species, the strength of these reactivations correlated with the magnitude of serial dependence in upcoming trials, and inducing prefrontal or premotor reactivations with transcranial magnetic stimulation increased serial dependence (Barbosa et al., 2020; de Azevedo Neto and Bartels, 2021).

Building on these findings, we previously proposed a specific mechanism for serial dependence alterations in schizophrenia and anti-NMDAR encephalitis (Stein et al., 2020).

In a computational cortical circuit model, we showed that a reduction of STP, potentially as a result of NMDAR dysfunction (Castro-Alamancos and Connors, 1996; Volianskis et al., 2013), resulted in reduced serial dependence (Stein et al., 2020). Here, we aim to test neurophysiological predictions of this model in EEG recordings in patients with anti-NMDAR encephalitis and schizophrenia, and in healthy subjects. Based on this computational model, we hypothesize that a reduction in STP should preclude neural reactivations in these patient populations during the ITI of the task. We first formalize our hypothesis in a circuit model of the prefrontal cortex with varying degrees of STP (Stein et al., 2020). We then test the prediction of reduced memory code reactivations in the ITI using multivariate EEG alpha power from our experimental populations. As hypothesized, ITI memory reactivations occur in healthy controls, but are absent in patients with anti-NMDAR encephalitis or schizophrenia. Based on single-trial decoding performance at the time of reactivation, we show that in healthy controls, but not in patients, reactivations are predictive of serial dependence strength in the upcoming trial. Finally, we use cross-decoders to show that memory codes, but not perceptual codes, are specifically impaired in patients. Thus, we provide specific evidence for reduced memory codes and memory reactivations in EEG as the neurophysiological correlates that underlie reduced serial dependence and the disruption of between-trial memory traces in patients with anti-NMDAR encephalitis and schizophrenia.

Results

STP modulates memory code reactivations in a circuit model

We used a computational network model that represents a cortical circuit with excitatory and inhibitory spiking neurons connected recurrently, and excitatory synapses endowed with STP dynamics. This circuit model has been used to simulate serial dependence in spatial working memory and derive the behavioral predictions of reduced STP (Stein et al., 2020). We now simulated again this model to derive neurophysiological predictions that could be tested in EEG data acquired in our patient groups. STP levels were chosen to mimic serial dependencies observed in patient populations as in ref (Stein et al., 2020). In this model, working memory representations are held in persistent delay firing (Fig. 1a). Delay activity induces potentiation of active excitatory synapses (Fig. 1b,c,d), which later biases attractively delay activity in the upcoming trial. Simulations with reduced levels of STP lead to a weaker enhancement of stimulus-specific synaptic traces (Fig. 1c,d). As done previously (Barbosa et al., 2020), to simulate memory reactivations in the ITI we delivered a non-specific excitatory drive to all neurons of the network (orange triangle in Fig. 1a,d). This drive might reflect external signals, such as the onset of the fixation dot, or internal preparatory signals, such as attention processes. In line with our previous results (Barbosa et al., 2020), memory codes were reactivated in some trials, leading to an increase in average firing rate tuning during the fixation period, before the onset of the next stimulus (Fig. 1d, black). In contrast, when STP was reduced (Fig. 1c,d, green and lilac), memory reactivations occurred less frequently (Fig. 1a, green and lilac). Albeit a small effect, weakening STP in our simulations also decreased the strength of memory codes during the delay (Fig. 1a), in line with previous findings (Kilpatrick, 2018; Seeholzer et al., 2019; Stein et al., 2021). Hence, our model predicts that reductions in STP should result in significantly reduced memory reactivations in the ITI in patients, compared to healthy controls.

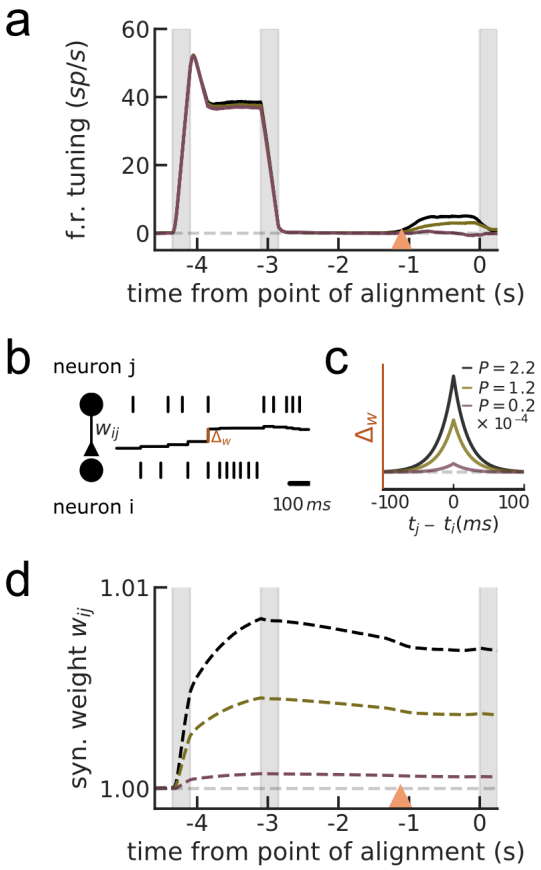

Fig. 1 | Reduced STP in a circuit model affects serial dependence and memory reactivations in the ITI

To test the impact of STP on serial dependence and memory reactivations, we simulated consecutive working memory trials in a network model that combines persistent delay activity and STP. **a** Firing rate tuning (calculated as the difference in average firing rates in 21 neurons centered at the presented stimulus value and 21 neurons centered at the opposite stimulus value). Firing rate tuning averaged over 1,000 trials. When stimuli in trial n-1 were presented at the neurons' preferred location, a subgroup of neurons represented the memory in a stable working memory code, discernible in firing rate tuning. Through the increase in synchronized firing, weights *w* were potentiated between delay-coactive neurons. After firing rates returned to spontaneous levels, firing rate tuning was lost, but synaptic weights remained potentiated until the onset of the next stimulus (see panel d). When a short, unspecific drive was delivered to all neurons in the network at -1.1 s, memory codes from the previous trial were recovered into neural tuning in some trials for networks with high- and intermediate STP levels, but not in networks with disrupted STP. **b** STP was implemented as an activity-dependent increase and decrease in synaptic weights between excitatory model neurons. The strength of each individual synapse is determined by w_{ij} (a, middle black trace), which is potentiated at each spike by an amount Δ_w that depends on the relative spike times t_j and t_i of pre- and postsynaptic neurons, respectively, and on the potentiation factor P and it is reduced by an amount relative to the synaptic strength at each presynaptic spike, resulting in activity-dependent decay. **c** Different potentiation factors P are chosen to represent reduced STP in anti-NMDAR encephalitis and schizophrenia. **d** Weight traces (averaged over 21 stimulus-selective neurons) in simulations with high (black), gradually reduced (green) and drastically reduced (lilac) values of potentiation factor *P*, as shown in b. Weight traces averaged over 1,000 trials, as in (a).

Decreased serial dependence and decreased memory reactivations in patients

To test this model prediction, we conducted a visuo-spatial working memory task (Fig. 2a) in 22 healthy controls, 27 patients with anti-NMDAR encephalitis, and 19 patients with schizophrenia. Note that behavioral results from a subset of 19 healthy controls, 16 patients with anti-NMDAR encephalitis, and 17 patients with schizophrenia were previously reported in ref (Stein et al., 2020). Patients with encephalitis had received immunotherapy and were in a progressive recovery phase, while patients with schizophrenia were tested during a stabilized period (Methods). In two sessions of 1.5 h each, subjects had to remember randomized angular locations at fixed eccentricity presented on a computer screen for short memory periods of 0, 1, or 3 s. After subjects indicated the memorized location in one trial with a mouse click, the next trial started after a self-paced ITI and a fixation period of 1.1 s (Methods, Fig. 2a). During the task, we recorded EEG activity in delay, response and fixation periods and analyzed these EEG data in relation to single-trial behavioral data.

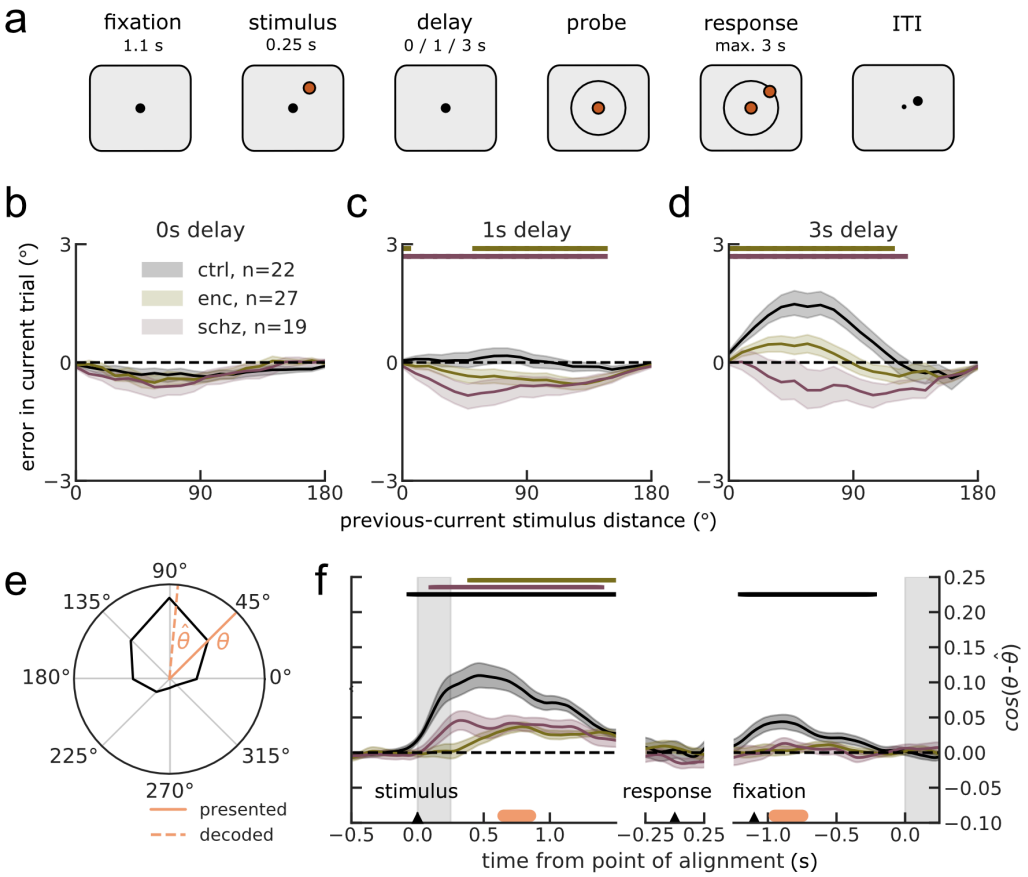

Fig. 2 | Decreased serial dependence and decreased memory code reactivations in patients

a In each trial, participants were asked to maintain eye fixation and the cursor position on a central fixation dot. After 1.1 s (fixation period), a stimulus appeared for 0.25 s at a randomly chosen angular location with fixed distance from the center. Delay lengths varied randomly between trials (0, 1 or 3 s), where 1 s trials were most frequent (66.7% of trials), and 0 and 3 s trials with equal probabilities (16.7% of trials). Subjects reported the remembered location with a mouse click and started the next trial by moving the mouse back to the fixation dot during the inter-trial-interval (ITI). **b-d**, Serial dependence by group and delay length. Serial dependence is calculated as the 'folded' error $\theta^{e\prime}$ for different θ^{d} (Methods). Shading, 32% bootstrap C.I. of the mean across participants for n = 22 healthy controls (ctrl), n = 19 patients with schizophrenia (schz), and n = 27 patients with anti-NMDAR encephalitis (enc). **b**, Serial dependence for all groups was repulsive in 0 s trials. **c** For 1 s trials, group differences in serial dependence emerged between ctrl and enc, and between ctrl and schz. **d** After 3 s delay, both patient groups showed drastically reduced biases compared to ctrl. Significance bars show significant permutation tests (1,000 permutations) at alpha = 0.05 between groups. **e** Decoding performance was calculated from the difference between predicted and presented angles, $(\theta - \hat{\theta})$. To this end, stimuli in the train and test set were binned into eight classes, and a tuning curve was reconstructed from test set neural activity (Foster et al., 2016). Decoding performance was then calculated as the cosine of the angular difference between the presented angle and the circular mean of this tuning curve $\hat{\theta}$ in the test trial. **f** Memory codes trained in mid-delay (0.65 - 0.85 s) were stable across large parts of the delay in trial n-1 (from stimulus presentation, S_{n-1}, to the response probe P_{n-1}), before disappearing around the time of response (R_{n-1}) and reemerging after the onset of fixation (F_n; upper significance bars, 1-sample cluster permutation test al alpha = 0.05). Lower significance bars indicate significant group differences between healthy controls and patients (two-sample cluster permutation test al alpha = 0.05). Shading, bootstrap s.e.m. across participants for n = 22 healthy controls (ctrl), n = 19 patients with schizophrenia (schz), and n = 27 patients with anti-NMDAR encephalitis (enc). Grey bars indicate stimulus and probe presentation, and orange bars indicate the timepoints referred to as "mid-delay" and "fixation".

As previously reported (Stein et al., 2020), patient populations had reduced delay-dependent serial dependence in this task (Fig. 2b,c,d). Serial dependence was calculated as the average distance of the memory report from the target, as a function of the distance between previous and current targets (Methods). Positive mean folded errors in these curves denote attraction to previous targets, while negative values denote repulsion (Barbosa and Compte, 2020). We observed small, repulsive biases for all groups in conditions with low memory requirements (0 s delay), potentially reflecting perceptual dependencies between trials (Fritsche et al., 2017). As expected (Fritsche et al., 2017), attractive biases in healthy controls increased gradually with working memory requirements. In contrast, biases remained repulsive for all delay lengths in patients with schizophrenia, and became only minimally attractive in encephalitis patients for 3 s delays. When comparing attractive biases between groups, memory-dependent serial dependence at 3 s delay was significantly reduced for encephalitis patients as well as patients with schizophrenia (Fig. 2d).

Electrophysiologically, we did not observe significant spectral differences in the frequency content of EEG signals recorded in the three groups during the task (Supplementary Fig. 1). However, our model made more specific predictions regarding the stimulus selectivity of EEG signals during the fixation period of the task, namely that group differences in memory code reactivations should occur during the ITI (Fig. 1a). To test this prediction, we used linear decoders to assess memory codes in EEG activity patterns. We extracted alpha power (8-12 Hz) from EEG signals at 43 scalp electrodes. The distribution of alpha power across electrodes is modulated by spatial attention and working memory, so that the location of memorized items can be read out with multivariate linear models during different task periods (Medendorp et al., 2007; Foster et al., 2016; Barbosa et al., 2020). For each subject, we trained a linear decoder on all but one trial and tested the predictive performance in the left-out trial (Fig. 2e, Methods). To compare the results with the predictions of our memory circuit model (Fig. 1), we specifically extracted (stable) memory codes, rather than perceptual or motor components of the EEG signal. Therefore, similar to our approach in ref. (Barbosa et al., 2020), we trained decoders on EEG data from the delay period (0.65 - 0.85 s), and tested whether this memory code would generalize to other task periods. In particular, we asked whether codes would be reactivated during the fixation period of the upcoming trial. Indeed, we found that memory codes for all three groups were stable during the memory delay and disappeared during the motor response (Fig. 2f, middle). In line with qualitative findings from our circuit model (Fig. 1d), memory codes during the delay were weaker in patients than in healthy controls (Fig. 2f, left), an effect that could not be explained by the lower number of trials (Supplementary Fig. 2) or by weaker modulations in the alpha band that was used for decoding (Supplementary Fig. 1). Finally, we tested whether memory codes would be reactivated during the pre-stimulus period of the next trial. Only in healthy controls, there was a significant reactivation of the memory code right after the onset of the fixation cross of the upcoming trial. As predicted by a model with reduced STP (Fig. 1a), we did not observe memory reactivations in patients. Together, both the reduction in serial dependence and the absence of memory reactivations during the ITI support the model-based hypothesis of disrupted STP in patients with anti-NMDAR encephalitis and in schizophrenia.

Memory code reactivations predict biases in the upcoming trial

Based on a previously reported relationship between memory reactivations and the strength of serial biases in the upcoming trial in healthy controls (Barbosa et al., 2020), we asked whether memory reactivations would be predictive of serial dependence on a within-subjects level. For each subject, we separated trials with high and low reactivations of the delay code during fixation (orange mark in rightmost panel of Fig. 2f), and calculated serial dependence separately for each set of trials (Methods). In Fig. 3a-c, we show the difference in averaged serial dependence Δ_{bias} between high- and low-decoding trials for each subject (Methods). Across participants, Δ_{bias} was positive in healthy controls, but non-significant (Fig. 3a). We wondered whether this relation was modulated by a difference in reactivation strength: In subjects whose memory code is not reactivated, a split based on decoding strength would separate trials mainly based on random fluctuations. We therefore correlated Δ_{bias} with the strength of memory reactivations for the three different groups ($cos(\theta - \widehat{\theta})$, see Methods). A linear regression model of Δ_{bias} as a function of *reactivation strength*, *group*, and their interaction confirmed our hypothesis: The higher the average reactivations, the more pronounced were differences between high- and low-decoding trials (*reactivation strength,* F(62,1) = 9.83, p = 0.003). Although the positive interaction between *reactivation strength* and *group* did not reach statistical significance (F(62,2) = 1.54, p = 0.22), groupwise correlations showed that the main effect of *reactivation strength* was driven mainly by healthy controls, whose reactivations were pronounced (Pearson's r = 0.60, p = 0.003; Fig. 3a), compared to patients with encephalitis (Fig. 3b; Pearson's r = 0.07, p = 0.75) and patients with schizophrenia (Fig. 3c; Pearson's r = 0.18, p = 0.47). To conclude, these results show that memory reactivations, as decoded from EEG alpha power, can increase serial dependence in subjects whose memory codes in the fixation period are reliably decoded. Together with the absence of memory reactivations and serial dependence in our patient groups, these findings confirm the predictions from our network model with reduced STP as a mechanistic interpretation of circuit alterations in anti-NMDAR encephalitis and schizophrenia.

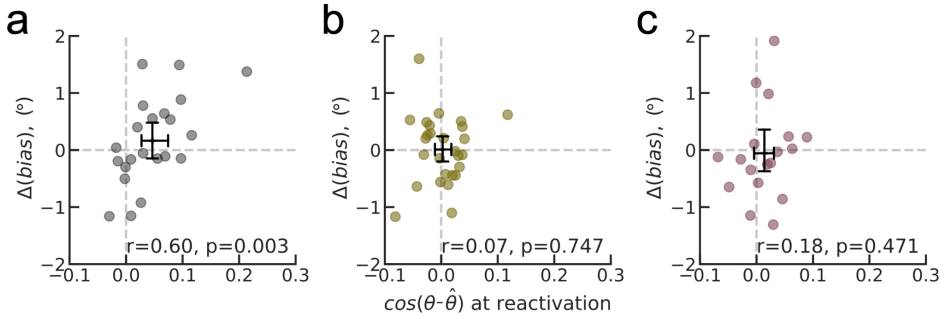

Fig. 3 | Memory code reactivations during ITI are predictive of serial dependence in subjects
a Difference Δ_{bias} in serial dependence between trials with high and low memory reactivations (Methods), as a function of the strength of memory reactivations. Δ_{bias} was positive, but non-significant in healthy controls (t = 1.00, p = 0.33), and increased with the overall strength of memory reactivations (Pearson's r = 0.60, p = 0.003). **b,c** Δ_{bias} was non-significant in both enc (t = 0.09, p = 0.93) and schz (t = -0.3, p = 0.76), and did not correlate with overall memory reactivation strength.

Finally, we asked whether single-trial differences in the memory code during the delay period would be predictive of inaccuracies in memory reports. For each subject, we separated trials into high-decoding and low-decoding trials, based on the predictive performance of the memory decoder in mid-delay (0.65 s to 0.85 s; Methods). We then calculated the difference between behavioral precision (measured as mean absolute difference between target and report) in high- and low-decoding trials. For all groups, this analysis revealed no relationship between decoding strength during delay and behavioral precision in single trials. Moreover, in line with our previous findings (Stein et al., 2020), based on behavior alone we did not find significant overall or delay-dependent impairments in precision between groups (*group*, $F(2,195) = 2.62$, $p = 0.75$; *group* × *delay*, $F(4,195) = 0.16$, $p = 0.96$, ANOVA). Together, this absence of a relationship between delay codes and working memory precision at both the group level and the intra-individual level suggests that the decoding of stimulus representations in our task is not causally linked with the precision of the memory readout, as detailed further in the discussion.

Working memory codes, but not perceptual components, are impaired in patients

We next asked whether differences in neural task representations between groups (Fig. 2f) would result from generally reduced decoding performance in patients, or whether differences in decoding performance were specific to the memory code. We thus used cross-temporal decoders (Stokes et al., 2013; King and Dehaene, 2014; Barbosa, 2017; Barbosa et al., 2020) (Fig. 4a-c) to disentangle temporal code components that could be related to different processing stages of the memory task. For each subject, we trained and tested decoders at all combinations of time points from 0.25 s before stimulus onset to the time of the response probe (1.25 s after the stimulus; Supplementary Fig. 3 shows cross-temporal decoding matrices for 3 s trials), and from 0.25 s before until 0.25 s after the motor response. For each group, we assessed temporal clusters of significant decoding across subjects (Fig. 4a-c, orange contours). Clusters differed in two aspects: First, we found apparent group differences in the overall decoding performance, especially during the delay period of the trial. In addition, we observed a reduced temporal stability of memory codes in both patients groups, as compared to healthy controls. While healthy controls' memory codes generalized across all time points of the delay, memory code generalization in patients was temporally more limited to adjacent time points.

This shows a clear difference in delay-period EEG decoding strength for the patient groups compared to the control group, but it does not clarify whether this is a result of a general reduction in decoding for all components of the task (stimulus encoding, memory maintenance, response). To answer this, we defined a decoder that contains all these components by training it in each period of the trial and testing it at the same timepoints in left-out trials (we term this kind of decoder a "dynamic" decoder). Spatial locations could be decoded throughout cue, delay and response periods in all three groups (Fig. 4d, upper significance bars). We then estimated the codes corresponding to sensory and motor processing by subtracting memory codes that we have defined before (Fig. 2, Fig. 4e) from these dynamic codes (Fig. 4d). We computed such "residual codes" for each subject, and compared them between groups of participants. The residual code revealed clear stimulus- and probe-related components, but it was virtually identical in patients and healthy controls (Fig. 4f), which is in striking contrast to the strong differences observed for the memory

code (Fig. 4e). Hence, we identified a specific decrease in EEG memory codes, but not visual or motor-related codes during the performance of our visuo-spatial working memory task in neuropsychiatric participants compared to healthy controls. This specificity underscores the significance of the finding of a lack of fixation-period reactivation codes in the patient groups (Fig. 2), as it cannot be explained merely on the basis of a general reduction of stimulus decoding performance in these participants.

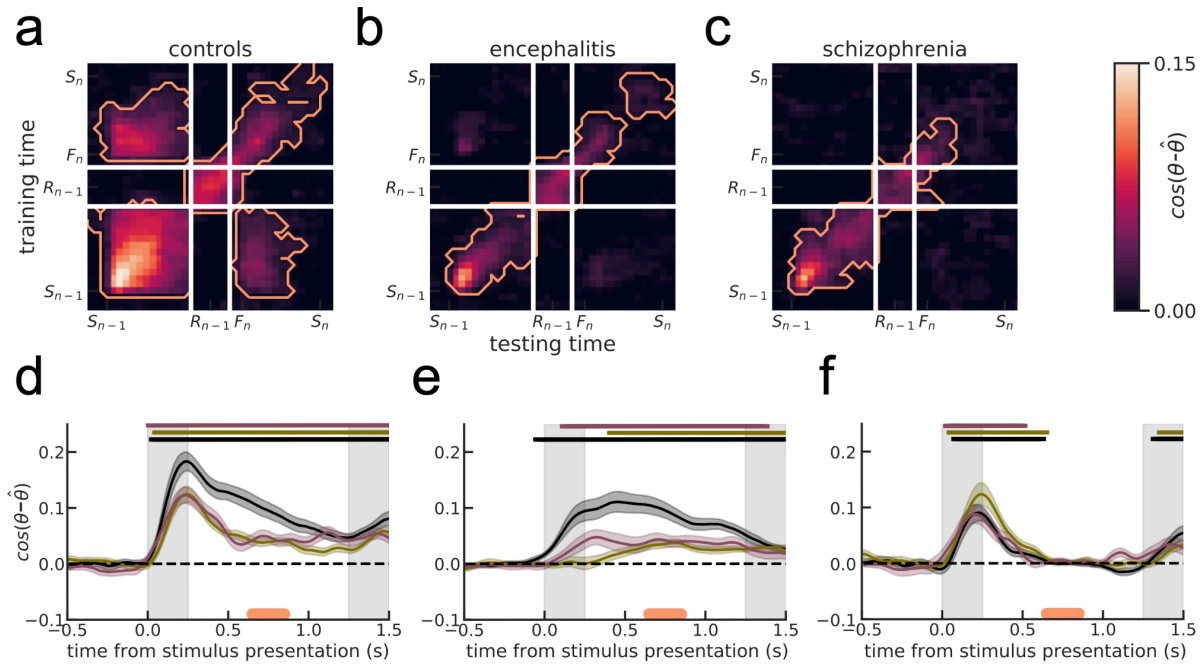

Fig. 4 | Working memory codes in patients are less reliable and less stable during delay

a,b,c Cross-temporal decoding during stimulus presentation (S), delay, response (R), and fixation (F) in successive trials (trials n-1 and n). White lines mark the discontinuity of EEG signals after the probe onset at 1.25 s. Orange lines mark significant decoding clusters (1-sample permutation test at alpha = 0.05). Spatial locations were decoded above chance at all time points comprising the diagonal for all groups. In controls, memory codes trained at any period of the delay generalized to any other delay time point, while in patients, memory codes did not generalize as extensively. During response, a different code component than during delay represented memory contents in all groups. **d,e,f** Dynamic codes (d) are weaker in patients than in healthy controls, resulting from a difference in memory codes trained in mid-delay (0.65-0.86 s, orange bar, (e)), while residual codes during stimulus presentation and memory recall (f) are comparable across groups. Spatial locations in working memory were decoded throughout the complete 1 s memory delay in all groups. The residual code was calculated by subtracting the delay component (middle) from the diagonal decoder (left). Shading, 32% bootstrap C.I. of the mean across participants for n = 22 healthy controls (ctrl), n = 19 patients with schizophrenia (schz), and n = 27 patients with anti-NMDAR encephalitis (enc); upper significance bars mark significant decoding, lower significance bars mark significant group differences, corrected with 1- or respectively 2-sample cluster permutation tests at alpha = 0.05. Gray bars indicate stimulus and probe presentation, and orange bars indicate the timepoints later referred to as “mid-delay” (0.65 s to 0.85 s). In all panels, we combine decoding results for 1 and 3 s trials up to 1 s after the stimulus offset (see Supplementary Fig. 3 for decoding performance only on 3 s delay trials).

Discussion

In this study, we assessed whether reduced serial dependence in anti-NMDAR encephalitis and schizophrenia would be reflected in neural reactivations of previous-trial memories during the inter-trial interval (ITI), as predicted by a cortical circuit model with defective short-term synaptic plasticity (STP). We tested this hypothesis with linear decoders trained on time-resolved alpha power in EEG. Moreover, we explored qualities of the working memory code during memory delays in patients, as compared to healthy controls. We showed that multivariate alpha power tracked memory contents in all groups. In patients with encephalitis and persons with schizophrenia, memory codes were selectively impaired when compared to healthy controls, and generalized less across time. In all groups, memory codes trained during the delay period disappeared completely during the response period. After the onset of the next trial, these codes reappeared in healthy controls, but not in patients. We reasoned that the reactivation of memory codes should be related to serial dependence, and confirmed this prediction in healthy controls: strong memory code reactivations during the fixation period were related to stronger serial bias in the upcoming trial. In contrast, we did not observe such a relationship in patients with encephalitis or schizophrenia, whose memory codes did not reactivate in the fixation period and were not predictive of biases.

Our findings confirm the relationship between working memory reactivations in the ITI and serial dependence (Barbosa et al., 2020), both on the group level, when comparing experimental groups with different degrees of serial dependence, and on the inter-individual level, when comparing healthy individuals with different serial dependence strength. Our computational modeling approach provides a mechanistic view of how code reactivations and serial dependence are connected: a memory trace of the previous trial is sculpted in subthreshold activity (in our model, synaptic weights modeled by STP) and exerts a pull on subsequent firing activity in the network, generating serial dependence. This same memory trace can be reactivated with a non-selective anticipatory input, and these code reactivations reinforce in turn the memory trace and enhance serial dependence (Barbosa et al., 2020). The correlation that we observed across individuals could then be interpreted in two different ways. Individuals could differ in the strength of memory traces (e.g. STP), and this would both impact serial dependence and the probability of memory reactivations. Alternatively, individuals could differ in their attentional mechanisms and thus their capacity to anticipate the task structure and generate reactivations that enhance serial dependence. In our previous study (Barbosa et al., 2020) we emphasized the latter mechanistic interpretation by focusing on within-subject comparisons where STP is presumably unchanged from trial to trial. In this study, we have instead been favoring the first interpretation (Fig. 1), but it should be noted that inter-individual variability in attentional mechanisms could also be implicated. Note, for instance, that patients with anti-NMDAR encephalitis presented a peculiar pattern, where serial dependence was reduced but not abolished, while code reactivations were completely absent. This pattern is precisely what our model would predict for the second interpretation, when deficits affect the attentional system: serial dependence can occur even without reactivations, only weaker than the biases generated when attentional mechanisms are able to trigger reactivations (Barbosa et al., 2020). Instead, the pattern observed in schizophrenia requires in our model a consistent reduction in memory traces in the ITI. As a consequence, serial dependence is completely

abolished. Thus, our model and data suggest two levels of deficits in these disorders: mechanisms of top-down control of working memory (impaired at least in anti-NMDAR encephalitis, but possibly also in schizophrenia), and subthreshold memory trace mechanisms of working memory (impaired at least in schizophrenia, but possibly also affected in anti-NMDAR encephalitis).

To confirm our model's mechanistic hypothesis that the interplay between persistent memory codes and NMDAR-dependent STP underlies serial dependence and explains the alterations observed in anti-NMDAR encephalitis and schizophrenia, further experimental work is needed in animal models. Combined electrophysiology and pharmacological studies could elucidate the relationship between NMDAR dysfunction, STP, memory reactivations and serial dependence. A recent in-vitro study has assessed the impact of patient-derived NMDAR antibodies on circuit physiology in the mouse hippocampus (Ceanga et al., 2023). Multiple effects were observed upon NMDAR blockade by antibodies, among which a pronounced modulation of STP. However, instead of reducing facilitation in excitatory synapses, as our model hypothesized, these experiments demonstrated reduced depression in inhibitory synapses. Although reduced facilitation of excitatory synapses may appear analogous to reduced depression of inhibitory synapses, explicit modeling of this manipulation is necessary to evaluate its computational impact. Of note, this study assessed the effects of NMDAR antibodies in the feedforward circuitry of CA1 in the hippocampus, and there could be differences with the strongly recurrent circuitry of the prefrontal cortex. Of particular interest will be pharmacological and neurophysiological studies in awake behaving animals to test the relationship between NMDAR-dependent mechanisms and serial dependence. While not as explicit as in-vitro studies, these experiments can also provide mechanistic insight of circuit-level NMDAR modulations through the assessment of rate modulations, neuron-pair cross-correlations and neural code reactivations (Barbosa et al., 2020). Experimental work would also be needed to discard an alternative explanation of our findings: Working memory codes could be held in one area during the delay, and transferred to another area after the response. From that area, stimulus-specific activity could be fed back to the memory circuit after the ITI, to then actively influence new, upcoming memories. This interpretation would be congruent with findings of ITI-, but not delay-representations in PPC in ref. (Akrami et al., 2018). In this view, a failure to reactivate memories in the fixation period could reflect the disrupted bi-directional communication between memory-maintaining circuits and brain areas that represent past memory contents during response or inter-trial periods.

Currently, we cannot fully explain why patients have weaker and less stable delay codes compared to healthy controls. Even if our network model simulations (Fig. 1a) and previous work (Kilpatrick, 2018; Seeholzer et al., 2019; Stein et al., 2021) show that reduced STP can lead to less stable memory codes, this effect should be weak, which does not quantitatively match our EEG results (Fig. 2f). Importantly, we discard that lower decoding performance during delay could reflect a reduced number of trials (Supplementary Fig. 2) or a reduction in univariate alpha power (Supplementary Fig. 1). In fact, alpha power during the delay was modulated more strongly in patients with encephalitis than in healthy controls (Supplementary Fig. 1). Intriguingly, we failed to find a relationship between delay code and working memory precision both on the inter-group level, and on the intra-individual level (between trials). In ref. (Stein et al., 2020), we have argued that intact memory precision in

patients might be explained through ceiling effects that emerge in the very simple working memory task performed in this study: subjects only needed to remember one item, during rather limited delay periods, while reduced working memory precision has been found in tasks with long delays (Starc et al., 2017) or more challenging stimuli (Hahn et al., 2018). In line with this reasoning, ref. (Driesen et al., 2008) have reported reduced memory-related BOLD signals in PFC and reduced memory precision in patients with schizophrenia in a task with long working memory delays. Nevertheless, a recent study that probed longer memory periods in a spatial working memory task revealed that, when factoring out serial dependence, the working memory precision deficits observed in patients with schizophrenia are small (Bansal et al., 2023). Thus, our task might not have tested the upper limits of working memory to identify the behavioral impact of the significant change in memory codes observed. Variability in response precision or in working memory decoding performance between trials or between individuals might not reflect a cognitively relevant dimension of our task.

To conclude, we identified a disruption in memory code reactivations during the ITI in anti-NMDAR encephalitis and in schizophrenia. We argued that reduced memory reactivations and reduced serial dependence observed in these patients are both related to a disruption in a subthreshold memory trace mechanism, such as STP, and possibly in top-down control mechanisms of working memory. To understand whether and how the absence of memory reactivations is related to NMDAR-dependent STP and to altered delay period memory codes, further work, ideally accompanied by electrophysiological recordings in the prefrontal cortex, is needed that specifically tests this hypothesis.

Acknowledgments

We acknowledge support from Institute Carlos III, Spain (Ref: PIE 16/00014), CELLEX Foundation, Edmond J. Safra Foundation, CERCA Programme/Generalitat de Catalunya, Generalitat de Catalunya (AGAUR 2014SGR1265, 2017SGR01565), “la Caixa” Foundation (ID 100010434, under the agreement LCF/PR/HR22-00221), and by the Spanish Ministry of Science, Competitiveness and Universities co-funded by the European Regional Development Fund (Refs: BFU 2015-65318-R, RTI2018-094190-B-I00). HS was supported by the “la Caixa” Banking Foundation (Ref: LCF/BQ/IN17/11620008), and the European Union’s Horizon 2020 Marie Skłodowska-Curie grant (Ref: 713673). JB was supported by the Bial Foundation (ref: 356/19). We thank the Barcelona Supercomputing Center (BSC) for providing computing resources. This work was developed at the buildings Centro Esther Koplowitz, CELLEX, and Hospital Clinic, Barcelona. We thank Thaís Armangue, Domingo Escudero, and Gisela Sugranyes for assistance in recruiting patients.

Methods

Experimental sample

We included n = 27 patients with anti-NMDAR encephalitis (enc; age 28.7 ± 11.3 years, mean ± s.d.; n = 5 male), n = 19 patients with schizophrenia or schizoaffective disorder (schz; age 21.3 ± 8.8 years, mean ± s.d.; n = 8 male), and n = 22 neurologically and psychiatrically healthy control participants (ctrl; age 24.9 ± 10.4 years, mean ± s.d.; n = 4 male), all with normal or corrected vision. Behavioral data from n = 19 controls, n = 16 patients with encephalitis, and n = 17 patients with schizophrenia has been reported before (Stein et al., 2020), and behavioral and EEG data from n = 14 healthy controls has been included in another previous study (Barbosa et al., 2020). Psychiatric diagnoses (or the absence thereof for controls) were confirmed using the Structured Clinical Interview for DSM IV (SCID-I) (First et al., 1996). Patients with anti-NMDAR encephalitis were recruited from centers in Spain (n = 25 in Spain), Germany (n = 1), and the United Kingdom (n = 1) and participated in the experiment several months after hospital discharge. Patients with anti-NMDAR encephalitis were diagnosed by confirmation of CSF IgG antibodies against the GluN1 subunit of the NMDAR (Graus et al., 2016). All healthy controls and patients with schizophrenia tested seronegative for antibodies against NMDAR in serum (Dalmau et al., 2008). Anti-NMDAR encephalitis is known to have a prolonged process of recovery after the acute stage of the disease (Titulaer et al., 2013), and patients in the prolonged recovery phase still suffer from cognitive deficits as has been previously described in cohorts with long follow-up (Finke et al., 2012). All patients were sufficiently recovered to participate in the testing procedure. Controls and patients with schizophrenia were recruited from the Barcelona area and from Hospital Clínic (Barcelona, Spain), respectively. Patients with schizophrenia were clinically stable at the time of testing. All participants (and, in the case of minors of age, their legal guardians) provided written informed consent and were monetarily compensated for their time and travel expenses, as reviewed and approved by the Research Ethics Committee of Hospital Clínic. All subjects were assessed for psychiatric symptoms and functionality through a battery of standard tests including the Spanish versions of the Positive and Negative Syndrome Scale (PANSS) (Kay et al., 1990), the Young Mania Rating Scale (YMRS) (Colom et al., 2002), the Hamilton Depression Rating Scale (HAM-D) (Ramos-Brieva and Cordero-Villafafila, 1988) and the Global Assessment of Functioning Scale (GAF) (Bobes et al., 2004). Furthermore, cognitive dysfunction in these patients has been longitudinally assessed with a battery of neuropsychology tests, revealing remarkable similarity of post-actue anti-NMDAR encephalitis and schizophrenia (Guasp et al., 2022).

Task protocol and behavioral testing

Participants completed two 1.5 h sessions performing a visuospatial working memory task described in Fig. 2a. In each session, participants were asked to complete 12 blocks of 48 trials. However, some participants did not complete all blocks, and some did not complete both sessions (on average, participants completed 1138.5 trials (median, ctrl, i.q.r. = 35.0), 1101.0 trials (median, enc, i.q.r. = 110.0), and 1017.0 trials (median, schz, i.q.r. = 301.0). For the stimulus presentation, we used Psychopy v3.1.5 on Python 2.7, running on a 17” HP ProBook laptop. Subjects were seated in a fixed position, using a chinrest, at a distance of 65 cm to the screen. Each trial began with the presentation of a central black fixation square on a gray background (0.5 x 0.5 cm) for 1.1 s. A single colored circle (stimulus, diameter 1.4 cm, 1 out of 6 randomly chosen colors with equal luminance) was then presented during 0.25 s at one of 360 randomly chosen angular locations at a fixed radius of 4.5 cm from the center. The stimulus was followed by a randomly chosen delay of 0 (16.67% of trials), 1 (66.67% of trials), or 3 s (16.67% of trials) in which only the fixation dot remained visible (except for 0 s trials, where the stimulus remained visible until the participant started to move the cursor). When the fixation dot changed to the stimulus color (probe), participants were asked to respond by making a mouse click at the remembered location (response). A white circle indicated the stimulus radial distance, so participants only had to remember the angular position. After the

response, the cursor had to be moved back to the fixation dot to start a new trial (ITI). Participants were instructed to maintain fixation during the fixation period, stimulus presentation, and memory delay and were free to move their eyes during response and when returning to the fixation dot.

Error and serial dependence analysis

Trial-wise response errors were measured as the angular distance between response and target. To exclude errors due to guessing or motor imprecision, we only analyzed responses within an angular distance of 1 radian and a radial distance of 2.25 cm from the stimulus. Further, we excluded trials in which the time of response initiation exceeded 3 s, and trials for which the time between the previous trial's response probe and the current trial's stimulus presentation exceeded 5 s. In total, 2.0% (median, ctrl, i.q.r. = 0.3%), 1.8% (median, enc, i.q.r. = 0.4%) and 2.0% (median, schz, i.q.r. = 0.3%) of trials per participant were rejected.

We quantified serial dependence as the error in the current trial as a function of the circular distance between the previous and the current trial's target location. Fig. 2b,c,d depict 'folded' serial dependence (Barbosa and Compte, 2020). Errors in single trials were multiplied by the sign of the previous-current distance in that trial, binned based on the previous-current distance, and averaged in sliding windows with size $\pi/3$ in steps of $\pi/20$. Positive mean folded errors should be interpreted as attraction towards the previous stimulus and negative mean folded errors as repulsion away from the previous location. In all figures including bias curves, s.e.m. are calculated across pooled trials from all subjects for each group and delay. For visualization, all values were transformed from radians to angular degrees.

EEG recordings and preprocessing

We recorded EEG from 43 electrodes attached directly to the scalp. The electrodes were placed according to the 10/10 International System. During the online acquisition, sites were referenced to an average of mastoids A1 and A2. Subsequently, the EEG was re-referenced offline to the common average reference. We further recorded horizontal EOG from both eyes, vertical EOG from an electrode placed below the left eye and ECG to detect cardiac artifacts. We used a Brainbox® EEG-1166 EEG amplifier with a .017-100 Hz bandpass filter and digitized the signal at 512 Hz using Deltamed Coherence® software (version 7) and BrainRT™ (version 2019).

EEG data was pre-processed using Fieldtrip (version 20171231) in MATLAB R2017b and R2019a. We excluded outlier trials in which variance or kurtosis across samples exceeded 4 standard deviations from mean variance or kurtosis over trials, respectively. To reduce artifacts in the remaining data, we ran an independent component analysis (ICA) on the trial-segmented data and corrected the signal for blinks, eye movements, and ECG signals, as identified by visual inspection of all components. Data were Hilbert-transformed (using the FieldTrip function "ft_freqanalysis.m") to extract frequencies in the alpha-band (8-12 Hz) and total power was calculated as the squared complex magnitude of the signal. Finally, we excluded trials in which lognormal alpha-power at any electrode exceeded the time-resolved trial average of lognormal alpha-power by more than 4 standard deviations, and trials in which the time-averaged variance across electrodes exceeded the mean variance over trials by more than 4 standard deviations (to increase the stability of trial-wise decoding predictions for different randomly chosen training sets). Excluding rejected trials and trials with 0 s delay, we used n = 900.63 ± 103.02 (ctrl, mean ± std); n = 870.44 ± 141.93 (enc, mean ± std); and n = 833 ± 153.33 (schz, mean ± std) trials per participant. To concatenate data from the two sessions for the same subject, we normalized each session's alpha-power for each electrode separately.

For time-frequency plots (Supplementary Fig. 1), we calculated the trial-averaged power in frequencies of interest between 2 – 40 Hz, from -3 s to 5 s relative to the time of stimulus presentation by applying a multitaper time frequency transformation with Hanning tapers (again using

the FieldTrip function “ft_freqanalysis.m”). Resulting power spectra were log transformed and averaged over electrodes. In Supplementary Fig. 1, we show power time-frequency plots, averaged over participants of each group (a-c), plots showing power modulations with respect to a pre-stimulus baseline (-0.5 s to 0 s relative to stimulus presentation, d-f), differences between group mean time-frequency plots (g,h), differences between baseline-corrected group mean time-frequency plots between groups (i,j). Contours show significant differences between groups in (g-j), tested by shuffling group labels 10.000 times and calculating confidence intervals for the difference in mean spectra. For (d-f), contours show significant modulations in power with respect to the pre-stimulus baseline, tested with bootstrapped confidence intervals over participants of the respective group. Contours result from Bonferroni-corrected comparisons at alpha = 0.05 (d-f) or alternatively, uncorrected comparisons at alpha = 0.05 (g-l).

EEG decoding

We used a linear decoder to read out the angular position of the stimulus from the distribution of alpha power across the 43 electrodes. We concatenated consecutive trials and trained the decoder on the stimulus label of the previous trial, to then decode location information throughout the previous and current trial. Trial-wise alpha power for each electrode was modeled as a linear combination of a set of regressors representing the stimulus location in the corresponding trial, $U = WM$, where *U* is a *J* × *K* matrix of alpha power measured at electrode *j* in trial *k*, *M* is the *N* × *K* design matrix of values for regressor *n* in trial *k*, and *W* is the *J* × *N* weight matrix, mapping the weight for regressor *n* to electrode *j*. *U* and *M* were given by the experiment, while *W* was fitted using least squares. The design matrix *M* is a set of eight regressors M_n representing expected values for feature *n* in trial *k (Brouwer and Heeger, 2009)*. The value of regressor M_n in trial *k* was determined as $sin(n\pi/8 - s_k\pi/8 + \pi/2)^7$, where s_k = [0…7] indicates which one of eight angular location bins (with width π/8 radians) included the stimulus shown in trial *k*.

We measured single-trial stimulus representations using leave-one-out cross-validation, ensuring an equal number of trials from each location bin in the training set (U_t and M_t). We estimated the weight matrix $\hat{W}$ and the design matrix M_k for the left-out trial *k*, as follows:

$$\hat{W} = U_t M_t^T (M_t M_t^T)^{-1}$$
$$\hat{M}_k = (\hat{W}^T \hat{W})^{-1} \hat{W}^T U_k$$

For each trial and time point, we repeated this analysis 10 times with randomly chosen training sets, and averaged *M* over all repetitions. Finally, we estimated the predicted angle $\hat{\theta}_k$ as the direction of the vector sum of feature vectors with length M_{nk} pointing at angular location bin centers $b_n = n\pi/8$ (n = 0…7). Trial-wise decoding strength was then defined as $cos(\hat{\theta}_k - \theta_k)$. To correlate the decoding strength with behavioral biases (Figs. 3), we increased the stability of trial-wise measures by training the decoder on temporally averaged data over a 200-ms window in mid-delay (0.65 - 0.85 s, orange mark in Fig. 2f). We then separated trials as high-decoding (>75th percentile) or low-decoding (<75th percentile) during delay (for correlations with memory precision) or respectively, during fixation (Fig. 3), and calculated the difference between absolute errors or respectively, between bias curves in each set of trials. The difference in bias strength between two groups of trials was calculated for previous-current distances between 0° and 90°, where biases are most prominent.

To explore the temporal generalization of the mnemonic and the response code over time, we trained decoders on the previous stimulus label in independent time windows of the previous and current trial, and tested them in all time points of previous delay, response and current fixation periods (from 0.25 s to 1.25 s after previous stimulus onset and from -0.25 s to 0.25 s after the previous response,

and -1.25 s to 0.25 s after the stimulus onset of the current trial; Fig. 4a-c). For decoding matrices, we averaged training and test data over independent windows of 50 samples (~97.77 ms). The high-resolution time course of the mnemonic code (Figs. 2f, 4d) was obtained by training the decoder on averaged data from 0.65 - 0.85 s after previous stimulus onset (dashed lines in decoding matrices), and by testing on averaged data from five samples (~9.77 ms) through consecutive trials. For all time series and cross-temporal matrices, significance was assessed with 1-sample or 2-sample cluster permutation tests (Maris and Oostenveld, 2007) with 1,000 permutations, implemented in the Python "mne" package (Gramfort et al., 2013).

Neural network simulations

We simulated consecutive pairs of trials in a spiking neural network model of prefrontal cortex implemented in Brian2 (Stimberg et al., 2019). $N_E = 1024$ excitatory and $N_I = 256$ inhibitory leaky integrate-and-fire neurons were connected all-to-all via synapses governed by NMDAR-, AMPAR-, and $GABA_A$R-dynamics, as described in ref. (Compte et al., 2000). All connection strengths of all-to-all connections were constant, except for recurrent excitatory connections, which were modulated depending on the distance in preferred location of presynaptic and postsynaptic neurons: $W_{ij}^{EE} = J(\theta_i - \theta_j)$, where J is a Gaussian function (centered at $\mu = 0$ with $\sigma = 14.4$ degrees) plus a constant, tuned so that $\sum_j J(\theta_i - \theta_j) = N_E$ and $J(0) = 1.63$. As a result, neurons with similar preferred locations had 1.63 stronger weights than the average weight. For equations describing network dynamics, please refer to ref. (Stein et al., 2020).

Moreover, connections between excitatory neurons were plastic (Fig. 1b): AMPAR and NMDAR synaptic variables w_{ij} characterize the synaptic weight between neuron *j* and neuron *i*. Upon synchronized pre- and postsynaptic spiking, w_{ij} was slightly enhanced by an amount Δ_w that depended on the relative spike times of neuron *j* and *i* to simulate an increase in probability of glutamate release (Volianskis et al., 2015):

$$w_{ij} = w_{ij} + \Delta_w(t_j - t_i) \geq 1.$$

The associative nature of this rule was determined by a potentiation function that required synchronization within a specific temporal window:

$$\Delta_w(t_j - t_i) = P \exp\left(-|t_j - t_i|/\tau_\Delta\right),$$

with potentiation factor P = 0.00022 (to simulate STP in healthy controls), P = 0.00012 (encephalitis), or P = 0.00002 (schizophrenia), and τ_Δ = 20 ms (Fig. 2b). Changes were sustained (did not decay with time), but synapses depotentiated based on presynaptic activity (Volianskis et al., 2013): at each presynaptic spike:

$$w_{ij} = w_{ij} - 0.04 * (w_{ij} - 1).$$

Dynamics in network connections are described in more detail in ref. (Stein et al., 2020). We simulated 1,000 pairs of consecutive trials with independent randomized stimulus locations. We then calculated rate tuning as the difference between firing rates of neurons selective for the presented location (in trial *k*-1) and neurons selective for the opposite location. Simulations started with a stimulus presentation at 0° (trial *k*-1) for 0.25 s. After the input was removed, a delay of 1 s followed. A negative input to the whole network during 0.25 s simulated the response and removed stimulus-associated neural activity. After an ITI of 2.75 s, a second stimulus (trial *k*) was delivered at a random location for 0.25 s. 1.1 s before the second stimulus, a transient excitatory drive (0.5 s) was delivered to all excitatory neurons in the network.

Bibliography

Akrami A, Kopec CD, Diamond ME, Brody CD (2018) Posterior parietal cortex represents sensory history and mediates its effects on behaviour. Nature 554:368–372.

Baddeley AD (1992) Working memory. Science 255:556–559.

Bae G-Y, Luck SJ (2019) Reactivation of previous experiences in a working memory task. Psychol Sci 30:587–595.

Bansal S, Bae G-Y, Robinson BM, Dutterer J, Hahn B, Luck SJ, Gold JM (2023) Qualitatively Different Delay-Dependent Working Memory Distortions in People With Schizophrenia and Healthy Control Participants. Biol Psychiatry Cogn Neurosci Neuroimaging 8:1218–1227.

Barbosa J, Compte A (2020) Build-up of serial dependence in color working memory. Sci Rep 10:10959.

Barbosa J, Stein H, Martinez RL, Galan-Gadea A, Li S, Dalmau J, Adam KCS, Valls-Solé J, Constantinidis C, Compte A (2020) Interplay between persistent activity and activity-silent dynamics in the prefrontal cortex underlies serial biases in working memory. Nat Neurosci 23:1016–1024.

Barbosa J (2017) Working memories are maintained in a stable code. J Neurosci 37:8309–8311.

Bliss DP, D'Esposito M (2017) Synaptic augmentation in a cortical circuit model reproduces serial dependence in visual working memory. PLoS ONE 12:e0188927.

Bobes J, Portilla MPG, Bascarán MT, Saiz PA, Bousoño M (2004) Banco de instrumentos básicos para la práctica de la psiquiatría clínica. Barcelona: Psiquiatría Editores S.L.

Brouwer GJ, Heeger DJ (2009) Decoding and reconstructing color from responses in human visual cortex. J Neurosci 29:13992–14003.

Castro-Alamancos MA, Connors BW (1996) Short-term synaptic enhancement and long-term potentiation in neocortex. Proc Natl Acad Sci USA 93:1335–1339.

Ceanga M, Rahmati V, Haselmann H, Schmidl L, Hunter D, Brauer A-K, Liebscher S, Kreye J, Prüss H, Groc L, Hallermann S, Dalmau J, Ori A, Heckmann M, Geis C (2023) Human NMDAR autoantibodies disrupt excitatory-inhibitory balance, leading to hippocampal network hypersynchrony. Cell Rep 42:113166.

Colom F, Vieta E, Martínez-Arán A, Garcia-Garcia M, Reinares M, Torrent C, Goikolea JM, Banús S, Salamero M (2002) [Spanish version of a scale for the assessment of mania: validity and reliability of the Young Mania Rating Scale]. Med Clin (Barc) 119:366–371.

Compte A, Brunel N, Goldman-Rakic PS, Wang XJ (2000) Synaptic mechanisms and network dynamics underlying spatial working memory in a cortical network model. Cereb Cortex 10:910–923.

Conway ARA, Kane MJ, Engle RW (2003) Working memory capacity and its relation to general intelligence. Trends Cogn Sci (Regul Ed) 7:547–552.

Dalmau J, Gleichman AJ, Hughes EG, Rossi JE, Peng X, Lai M, Dessain SK, Rosenfeld MR, Balice-Gordon R, Lynch DR (2008) Anti-NMDA-receptor encephalitis: case series and analysis of the effects of antibodies. Lancet Neurol 7:1091–1098.

Dalmau J, Tüzün E, Wu H, Masjuan J, Rossi JE, Voloschin A, Baehring JM, Shimazaki H, Koide R, King D, Mason W, Sansing LH, Dichter MA, Rosenfeld MR, Lynch DR (2007) Paraneoplastic anti-N-methyl-D-aspartate receptor encephalitis associated with ovarian teratoma. Ann Neurol 61:25–36.

de Azevedo Neto RM, Bartels A (2021) Disrupting Short-Term Memory Maintenance in Premotor

Cortex Affects Serial Dependence in Visuomotor Integration. J Neurosci 41:9392–9402.

Driesen NR, Leung H-C, Calhoun VD, Constable RT, Gueorguieva R, Hoffman R, Skudlarski P, Goldman-Rakic PS, Krystal JH (2008) Impairment of working memory maintenance and response in schizophrenia: functional magnetic resonance imaging evidence. Biol Psychiatry 64:1026–1034.

Eckert A-L, Gounitski Y, Guggenmos M, Sterzer P (2023) Cross-Modality Evidence for Reduced Choice History Biases in Psychosis-Prone Individuals. Schizophr Bull 49:397–406.

Finke C, Kopp UA, Prüss H, Dalmau J, Wandinger K-P, Ploner CJ (2012) Cognitive deficits following anti-NMDA receptor encephalitis. J Neurol Neurosurg Psychiatr 83:195–198.

First MB, Spitzer RL, Gibbon M, Williams JBW (1996) Structured Clinical Interview for DSM-IV Axis I Disorders, Clinician Version (SCID-CV). Washington, D.C.: American Psychiatric Press, Inc.

Foster JJ, Sutterer DW, Serences JT, Vogel EK, Awh E (2016) The topography of alpha-band activity tracks the content of spatial working memory. J Neurophysiol 115:168–177.

Fritsche M, Mostert P, de Lange FP (2017) Opposite effects of recent history on perception and decision. Curr Biol 27:590–595.

Funahashi S, Bruce CJ, Goldman-Rakic PS (1989) Mnemonic coding of visual space in the monkey's dorsolateral prefrontal cortex. J Neurophysiol 61:331–349.

Gold J, Bansal S, Robinson B, Anticevic A, Luck SJ (2023) Opposite direction spatial working memory biases in people with schizophrenia and healthy controls. PsyArXiv https://doi.org/10.31234/osf.io/2kdje

Goldman-Rakic PS (1994) Working memory dysfunction in schizophrenia. J Neuropsychiatry Clin Neurosci 6:348–357.

Goldman-Rakic PS (1995) Cellular basis of working memory. Neuron 14:477–485.

Gramfort A, Luessi M, Larson E, Engemann DA, Strohmeier D, Brodbeck C, Goj R, Jas M, Brooks T, Parkkonen L, Hämäläinen M (2013) MEG and EEG data analysis with MNE-Python. Front Neurosci 7:267.

Graus F et al. (2016) A clinical approach to diagnosis of autoimmune encephalitis. Lancet Neurol 15:391–404.

Guasp M et al. (2022) Clinical characterisation of patients in the post-acute stage of anti-NMDA receptor encephalitis: a prospective cohort study and comparison with patients with schizophrenia spectrum disorders. Lancet Neurol 21:899–910.

Hahn B, Robinson BM, Leonard CJ, Luck SJ, Gold JM (2018) Posterior parietal cortex dysfunction is central to working memory storage and broad cognitive deficits in schizophrenia. J Neurosci 38:8378–8387.

Hajonides JE, van Ede F, Stokes MG, Nobre AC, Myers NE (2023) Multiple and Dissociable Effects of Sensory History on Working-Memory Performance. J Neurosci 43:2730–2740.

Javitt DC (2010) Glutamatergic theories of schizophrenia. Isr J Psychiatry Relat Sci 47:4–16.

Kay SR, Fiszbein A, Vital-Herne M, Fuentes LS (1990) The Positive and Negative Syndrome Scale--Spanish adaptation. J Nerv Ment Dis 178:510–517.

Kilpatrick ZP (2018) Synaptic mechanisms of interference in working memory. Sci Rep 8:7879.

King JR, Dehaene S (2014) Characterizing the dynamics of mental representations: the temporal generalization method. Trends Cogn Sci (Regul Ed) 18:203–210.

Kiyonaga A, Scimeca JM, Bliss DP, Whitney D (2017) Serial Dependence across Perception, Attention, and Memory. Trends Cogn Sci (Regul Ed) 21:493–497.

Maris E, Oostenveld R (2007) Nonparametric statistical testing of EEG- and MEG-data. J Neurosci Methods 164:177–190.

Medendorp WP, Kramer GFI, Jensen O, Oostenveld R, Schoffelen J-M, Fries P (2007) Oscillatory activity in human parietal and occipital cortex shows hemispheric lateralization and memory effects in a delayed double-step saccade task. Cereb Cortex 17:2364–2374.

Olney JW, Newcomer JW, Farber NB (1999) NMDA receptor hypofunction model of schizophrenia. J Psychiatr Res 33:523–533.

Ramos-Brieva JA, Cordero-Villafafila A (1988) A new validation of the Hamilton Rating Scale for Depression. J Psychiatr Res 22:21–28.

Seeholzer A, Deger M, Gerstner W (2019) Stability of working memory in continuous attractor networks under the control of short-term plasticity. PLoS Comput Biol 15:e1006928.

Sheehan TC, Serences JT (2022) Attractive serial dependence overcomes repulsive neuronal adaptation. PLoS Biol 20:e3001711.

Starc M, Murray JD, Santamauro N, Savic A, Diehl C, Cho YT, Srihari V, Morgan PT, Krystal JH, Wang X-J, Repovs G, Anticevic A (2017) Schizophrenia is associated with a pattern of spatial working memory deficits consistent with cortical disinhibition. Schizophr Res 181:107–116.

Stein H, Barbosa J, Compte A (2021) Towards biologically constrained attractor models of schizophrenia. Curr Opin Neurobiol 70:171–181.

Stein H, Barbosa J, Rosa-Justicia M, Prades L, Morató A, Galan-Gadea A, Ariño H, Martinez-Hernandez E, Castro-Fornieles J, Dalmau J, Compte A (2020) Reduced serial dependence suggests deficits in synaptic potentiation in anti-NMDAR encephalitis and schizophrenia. Nat Commun 11:4250.

Stimberg M, Brette R, Goodman DF (2019) Brian 2, an intuitive and efficient neural simulator. eLife 8.

Stokes MG, Kusunoki M, Sigala N, Nili H, Gaffan D, Duncan J (2013) Dynamic coding for cognitive control in prefrontal cortex. Neuron 78:364–375.

Titulaer MJ, McCracken L, Gabilondo I, Armangué T, Glaser C, Iizuka T, Honig LS, Benseler SM, Kawachi I, Martinez-Hernandez E, Aguilar E, Gresa-Arribas N, Ryan-Florance N, Torrents A, Saiz A, Rosenfeld MR, Balice-Gordon R, Graus F, Dalmau J (2013) Treatment and prognostic factors for long-term outcome in patients with anti-NMDA receptor encephalitis: an observational cohort study. Lancet Neurol 12:157–165.

Volianskis A, Bannister N, Collett VJ, Irvine MW, Monaghan DT, Fitzjohn SM, Jensen MS, Jane DE, Collingridge GL (2013) Different NMDA receptor subtypes mediate induction of long-term potentiation and two forms of short-term potentiation at CA1 synapses in rat hippocampus in vitro. J Physiol (Lond) 591:955–972.

Volianskis A, France G, Jensen MS, Bortolotto ZA, Jane DE, Collingridge GL (2015) Long-term potentiation and the role of N-methyl-D-aspartate receptors. Brain Res 1621:5–16.

Wang XJ (1999) Synaptic basis of cortical persistent activity: the importance of NMDA receptors to working memory. J Neurosci 19:9587–9603.

Zhang H, Luo H (2023) Feature-specific reactivations of past information shift current neural encoding thereby mediating serial bias behaviors. PLoS Biol 21:e3002056.

Supplementary Material

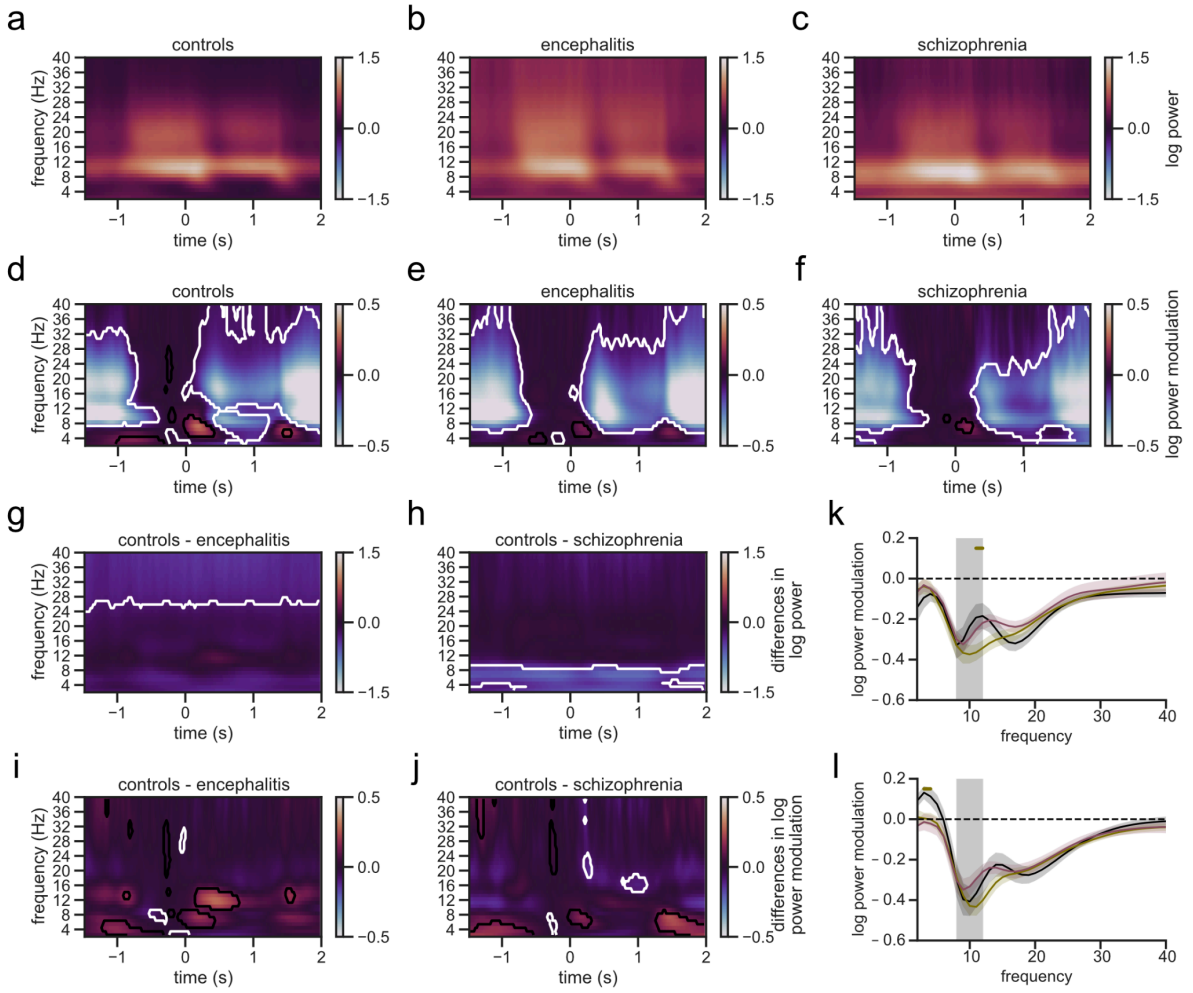

Supplementary Fig. 1 | Alpha power is not modulated less efficiently in patients than in healthy controls

We tested whether decreased decoding performance in patients could be an effect of a less efficient modulation of alpha power during working memory delays. We decomposed EEG signals at each electrode into different frequency bands using a multi-taper-method convolution (with fieldtrip function “mtmconvol”) with Hanning tapers, and log-transformed resulting time-frequency spectra. **a-c**, log power spectra for each group show strong power on the alpha band during pre-stimulus, stimulus presentation, and delay. **d-f**, To assess the significance of power modulations during the active task period, we subtracted the average pre-stimulus log power (-0.5 - 0 s) from each log power spectrum. All three groups show a significant modulation of spectral log power across a wide range of frequencies (white contours, significant decrease; black contours, significant increase w.r.t. baseline, bootstrap resampling test at alpha = 0.05, Bonferroni-corrected for multiple comparisons) after stimulus onset and in the pre-stimulus period. **g,h**, When comparing power between groups, higher alpha power during the task period did not reach significance either for ctrl vs. enc (e), nor for ctrl vs. schz (h), 2-sample permutation test at alpha = 0.05 (uncorrected). **i,j**, Similarly, differences in alpha power modulation with respect to baseline did not reach significance either for ctrl vs. enc (e), nor for ctrl vs. schz (h), 2-sample permutation test at alpha = 0.05 (uncorrected). A qualitative effect of stronger alpha power decreases is observed for the inter-trial interval. **k,l**, Both during delay (0.5 - 1.0 s after stimulus presentation) and fixation periods (-1.1 – -0.6 s pre-stimulus), there is no difference in relative power between ctrl and schz, even under an uncorrected alpha = 0.05. 2-sample permutation test on average power across subjects. Gray bars indicate the alpha band, which was used in the decoding procedure; error shading depicts +/- 1 s.e.m. (over subjects in each group).

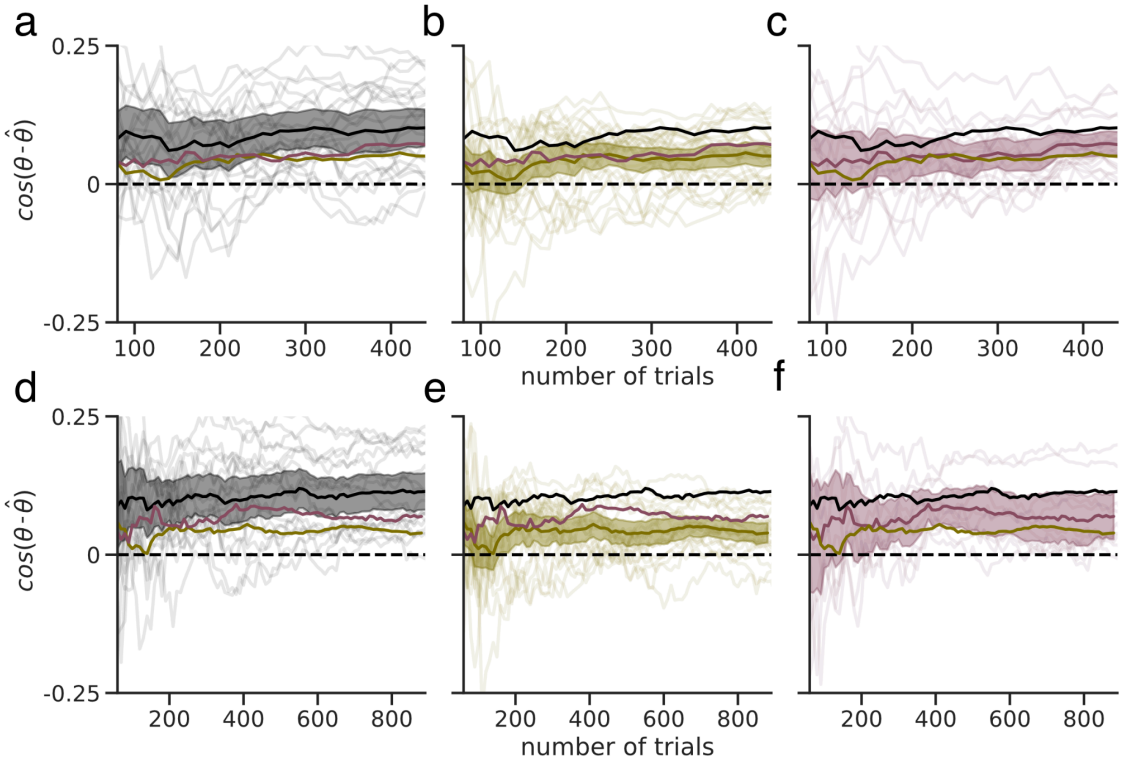

Supplementary Fig. 2 | Decoding performance as a function of the number of trials

To understand whether reduced memory codes in patients were related to the lower average number of trials in patients (number of trials: ctrl, n = 900.63 ± 103.02; enc, n = 870.44 ± 141.93; schz, n = 833 ± 153.33), we measured the increase in decoding performance when including increasing numbers of trials. For each subject (transparent lines), we trained and tested decoders in mid-delay (0.65 - 0.85 s after stimulus onset) on the first *n* trials of a session (x-axis). **a-c** The upper row shows the increase in decoding performance in all participants, up to the minimum number of trials (n=440 trials) that any included subject had performed (ctrl, n = 22; enc, n = 27; schz, n = 19). **d-e** The lower row shows the increase in decoding performance in a subset of subjects (ctrl, n = 19; enc, n = 21; schz, n = 10) who had performed the full experiment (after excluding trials during preprocessing, the cutoff was set to n = 880 trials). Left (black), healthy controls, middle (green), encephalitis, right (purple), schizophrenia. In all groups, mean decoding performance across subjects increased when including more trials, but saturated at ~ 400 trials. Importantly, group differences remained marked when fixing the number of trials along the entire x-axis. Shading, 95% bootstrap C.I.

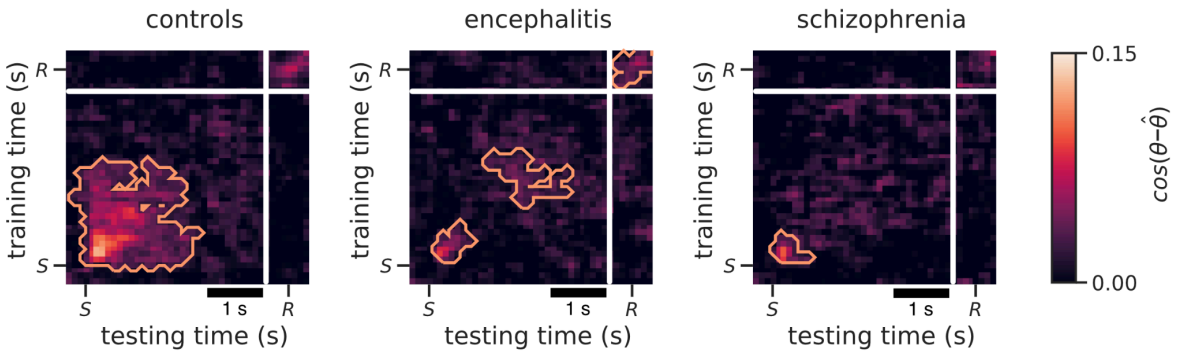

Supplementary Fig. 3 | Cross-temporal decoding in 3 s delay trials

Cross-temporal decoding during stimulus presentation (S), delay, and response (R), trained and tested only on 3 s trials. Compare to Fig. 3d-f, where decoders were trained on pooled 1 and 3 s trials. White lines mark the discontinuity of EEG signals after the probe onset at 3.25 s. Orange lines mark significant decoding clusters (1-sample permutation test at alpha = 0.05). Spatial locations were decoded above chance from ~0 - 2 s after stimulus onset in healthy controls. In patients, using only 3 s trials impaired decoding performance more dramatically, so that locations could only be decoded reliably around the time of stimulus presentation, and weakly around ~2 s for patients with encephalitis.